The study of the Urban Heat Island effect in Cyprus using Google Earth Engine for 2013-2023

Charalampos Soteriades[b], Stelios P. Neophytides*[a,b], Silas Michaelides [a], Diofantos G. Hadjimitsis[a,b]
[a]ERATOSTHENES Centre of Excellence, Franklin Roosevelt 82, 3012, Limassol, Cyprus.
[b]Department of Civil Engineering and Geomatics, Cyprus University of Technology, Archiepiskopou Kyprianou, 3036, Limassol, Cyprus.
*stelios.neophytides@eratosthenes.org.cy

ABSTRACT

The process of urbanization in Cyprus has been rapidly enhancing in the last 35 years, affecting the local climate. The contrast between energy absorption in developed urban areas and surrounding rural areas results in a differentiation of the local climate. The monitoring, therefore, of the urban heat island effect in main urban areas is essential, as data from a systematic examination can be of vital importance to policy makers and can assist them in adopting appropriate mitigation strategies and improve overall urban planning. The current study presents the results of the Urban Heat Island effect on the main cities in Cyprus (Paphos, Limassol, Larnaca and Nicosia) using Remote Sensing through Google Earth Engine. Data analytics techniques identify the correlation between different satellite indices and the Urban Heat Island phenomenon. The percentage of green coverage and the density of buildings have been identified as the main cause of the phenomenon. Findings from the study can be of use to local authorities to support their proposed revisions of local planning.

Keywords: Remote sensing, urban heat island, vegetation cover, urban areas, correlation

1. INTRODUCTION

Currently, more than 50% of people on Earth reside in cities, and by 2050, this percentage is predicted to rise to 11.66%, particularly in developing nations. Rapid urbanization is largely to blame for environmental issues, as it seems to have an impact on the urban climate. Heat and albedo are impacted by changes in land surface properties brought about by changes in land use/land cover (LULC). As a result, rising air and surface temperatures, along with variations in other climate factors like humidity and rainfall, all influence the urban climate. The urban heat island (UHI) phenomenon is one of the most prevalent environmental problems that cities have to deal with today. This is the term used to describe the rise in temperature (air and surface) in an urban area relative to the surrounding rural areas. As a consequence of LULC changes which are affecting urban climate, the UHI phenomenon has drawn a lot of caution.

An examination was conducted on surface thermal pattering through land cover thermal response for the Salt Lake City, Utah, USA study area at two scales: 1) community level and 2) regional or valley level. Data from the Advanced Thermal and Land Applications Sensor (ATLAS) airborne sensor, a high spatial resolution (10m) dataset suitable for an environment containing a concentration of different land covers, was exploited for both land cover and thermal analysis in community level[1].

Hadjimitsis et al. [2]examined the urban heat island phenomenon in Cyprus based on both multi-temporal satellite and meteorological data. The synoptic conditions favoring the development of heat wave events were discussed. Neutral network analysis was used to classify summary patterns and correlate them with heat events.

An analysis on the spatiotemporal variations of urban heat island (UHI) in Hangzhou using multisource remote sensing data was conducted. The annual human settlement index (HSI) was derived from the annual MODIS NDVI and DMSP-OLS datasets from 2000 to 2013 [3].

Kaplan [4]. examined the roles of greenery and building areas in reducing surface UHI using remote sensing data. To investigate this role of residential and green areas, satellite data from Landsat ETM+ was used to analyze land surface temperature and data from the high-resolution Planet Scope DOVE to analyze residential and green areas

Tenth International Conference on Remote Sensing and Geoinformation of the Environment (RSCy2024), edited by A. Christofe, S. Michaelides, D. Hadjimitsis, C. Danezis, K. Themistocleous, N. Kyriakides, G. Schreier,
Proc. of SPIE Vol. 13212, 132121F · © 2024 SPIE · 0277-786X · doi: 10.1117/12.3037670

Over a 14-year period, researchers used remote sensing data to track the evolution of the UHI phenomenon, as well as the Google Earth engine, in the city of Chennai, India. Google Earth was used to process the large volume of data available in a reasonable amount of time[5].

In the present study, to investigate the UHI phenomenon, we used remote sensing data to characterize surface temperature at the neighborhood level. Previously, land surface temperature data from Landsat 8 and the MODIS sensor on the Aqua and Terra satellites were compared to data from five urban areas in a New York City neighbourhood [6]. The effect of building thermal anisotropy on the surface UHI phenomenon in Beijing was investigated, with a focus on roof temperature. Surface UHI have been calculated using roof and surface temperatures, respectively[7]. ASTER imagery was used to model UHI and its relationship with impervious surfaces and greenness. In their research, a kernel convolution modelling method for 2-D land surface images was extended to characterize and model the UHI in Indianapolis as a Gaussian process[8].

The main aim of this work is to determine whether Urban Heat Islands (UHI) exist in Cyprus' cities and rural areas based on space-based observations in the decade 2013-2023. Furthermore, in order to contribute to sustainable urban development practices and offer insights into possible mitigation techniques, we also wish to investigate the relationship between the vegetation cover and the intensity of the urban heat island. The rest of the paper is structured as follows. Section 2 describes the methodology followed for the correlation assessment. Moreover, Section 2 describes the data and vegetation indices used in this study. Section 3 gives an overview of the results. Finally, Section 4 concludes this work.

2. MATERIALS AND METHODS

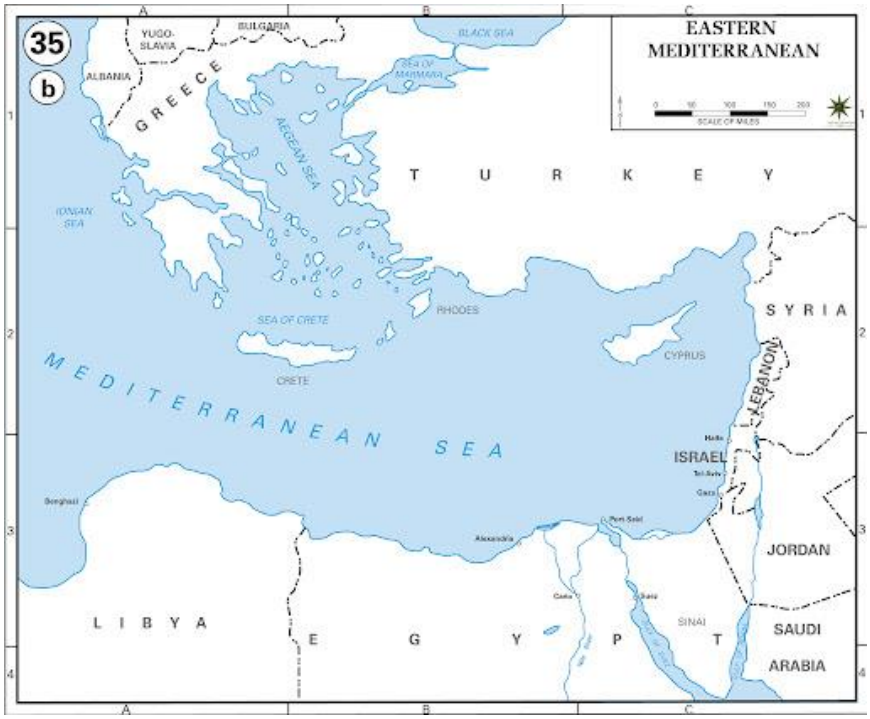

Fig. 1. Map of Easter Mediterranean

Case study

Cyprus is an island situated in the eastern Mediterranean Sea as shown in Fig. 1, and is part of the wider area of the Eastern Mediterranean, Middle East and North Africa (EMMENA) region[9]. With a total area of 9254 km^2, the island has a semi-arid climate that experiences frequent droughts. Furthermore, it is noted that Cyprus' climate exhibits a varying spatiotemporal behavior due to the various topographic features brought about by the island's complex terrain. Cyprus experiences typical Mediterranean summers that are hot and dry and mild winters that are rainy. Urbanization, changes in land use, and alteration of natural land cover are the main drivers of UHI in Cyprus. Natural vegetation is replaced by impermeable surfaces like concrete and asphalt when cities grow, which results in less evaporative cooling and more heat

absorption. The fast growth of Cyprus' cities (Paphos, Limassol, Nicosia, Larnaca) has led to changes in land use and increased urban congestion.

Data collection

NASA's Landsat-8 satellite data covers the years from 2013 through 2023 acquired for this investigation through Google Earth Engine[10]. The imagery was collected annually between May 1st and September 30th, with an emphasis on the warmest months to capture the summer-time phenomena known as the Urban Heat Island (UHI). To assure data accuracy, cloud and cloud shadows were masked using the Landsat Surface Reflectance Quality Assessment (QA) band. Cloud and cloud shadows can drastically alter temperature readings and spectral index computations. Before processing, scaling factors were applied to the Landsat-8 images to guarantee the data's accuracy and comparability. For both optical and thermal bands, these scaling factors translate digital numbers (DN) to physical units.

The scale factors applied were 0.0000275 and -0.2 for optical bands and 0.00341802 and 149.0 for thermal bands, respectively. Landsat 8 images acquired using Google Earth Engine.

Thermal and vegetation indices were computed using data from the Landsat-8 satellite. In order to evaluate vegetation cover and to conduct a correlation analysis between the intensification of UHI and vegetation in urban and rural areas, the Normalized Difference Vegetation Index (*NDVI*) which is denoted in Eq. 1, and Fraction of Vegetation Cover (*FV*) which is denoted in Eq. 2, were employed. Furthermore, to evaluate surface temperature changes and quantify the intensity of UHI which is defined in Eq. 5, thermal indices such as Emissivity (*EM*) and Land Surface Temperature (*LST*) defined in Eqs. 3 and 4, respectively, were calculated. Moreover, another index was calculated for the assessment, namely, the Urban Thermal Field Variance Index (*UTFVI*), which is defined in Eq. 6. These indices offer vital insights into urban microclimates and can be used as input in the drafting of urban planning strategies.

NDVI is a popular vegetation index which is used to determine the health and the growth of vegetation in an area of interest:

$$NDVI = \frac{(NIR - Red)}{(NIR + Red)} \ (1),$$

Where, *NIR* is the Near-Infrared band and *Red* is the Red band of Landsat-8.

FVC is a proxy of *NDVI* which is important in determining the vegetation of cover in a study area:

$$FVC = \left(\frac{NVDI - NVDI_{min}}{NVDI_{max} - NDVI_{min}}\right) \ (2),$$

Where, *NDVI* is the *NDVI* at the current pixel, $NDVI_{min}$ is the minimum observed *NDVI* value in an area of interest, and $NDVI_{max}$ is the maximum observed *NDVI* value in an area of interest.

Emissivity is defined as the ratio of energy radiated from a material's surface to that radiated from a perfect emitter.

Satellite *EM* is a proxy of the composition of the surface materials in the area of interest:

$$EM = 0.004 \times FVC + 0.986 \ (3),$$

Where, *FVC* is the Fraction of Vegetation Cover as calculated by Eq. 2.

LST is the satellite-based Land Surface Temperature:

$$LST = \frac{T_b}{1 + \left(0.00115 \times \frac{T_b}{0.48359547432}\right) \times \log(EM)} - 273.15 \ (4),$$

where T_b represents the temperature acquired from the thermal band of Landsat-8 and *EM* is the Emissivity calculated by Eq. 3.

$$UHI = \frac{LST - LST_{mean}}{LST_{std}} \quad (5),$$

where LST_{mean} is the mean *LST* and LST_{std} is the standard deviation of *LST* of study area.

UTFVI is often used to assess the thermal quality of urban areas,

$$UTFVI = \frac{LST - LST_{mean}}{LST} \quad (6),$$

where LST_{mean} is the mean *LST* and *LST* as calculated by Eq. 4.

Moreover, air temperature measurements at 1.2 meters were collected from the open-access archive of Department of Meteorology of Cyprus in the major cities of Cyprus. These measurements were collected for investigating temperature fluctuations during the summer period, providing valuable data for understanding urban heat island effects and as inputs to the design of strategies for climate resilience and adaptation in urban areas.

Correlation analysis

The linear relationships between the variables are measured by Pearson correlation which is defined by Eq. 7. When the value is near to +1, a strong positive linear relationship is indicated; when the value is near to -1, a strong negative linear relationship is indicated. When the value is zero, a little to no linear relationship is indicated. On the other hand, monotonic relationships between the variables are measured by Spearman correlation which is calculated by equation 8. As long as there is a consistent general trend, the statistical methodology is unaffected by a constant (linear) increase or decrease. When the value number is approaching +1, a positive monotonic trend is shown; when the number is approaching -1, a negative monotonic trend is shown. When the value number is close to zero, a little to no monotonic relationship is suggested.

$$r = \frac{\Sigma\,(x_i - \overline{x})\,(y_i - \overline{y}\,)}{\sqrt{\sum(x_i - \bar{x})^2 \sum(y_i - \bar{y})^2}} \quad (7),$$

where r is the Pearson correlation coefficient, x_i are the values of *x*-variable in a sample, $\bar{x}$ are the mean values of *x*-variable, y_i is the is the value of *y*-variable in the sample and $\bar{y}$ is the mean value of the *y*-variable.

$$\rho = 1 - \frac{6\,\sum d_i^2}{n\,(n^2 - 1)} \quad (8),$$

where ρ is the Spearman's rank correlation coefficient, the d_i is the observation differences between the two ranks and n is the number of observations.

3. RESULTS

The highest temperatures in each year within the decade 2013 to 2023 recorded in the four significant Cypriot cities (i.e., Paphos, Limassol, Nicosia, and Larnaca) are shown in Fig. 2. The cities with the highest average maximum temperatures are Nicosia, Limassol, and Paphos. Over the course of the observation period, Larnaca exhibits the lowest maxima. All four cities exhibit a general upward trend in maximum temperatures, despite annual fluctuations. When comparing the maximum temperatures in 2013 (which were roughly 20ºC) to those of 2023 (which were closer to 30 ºC) this trend

becomes especially evident. Moreover, the warmest day in Cyprus during 2013 to 2023 was recorded in Nicosia, with more than 40°C.

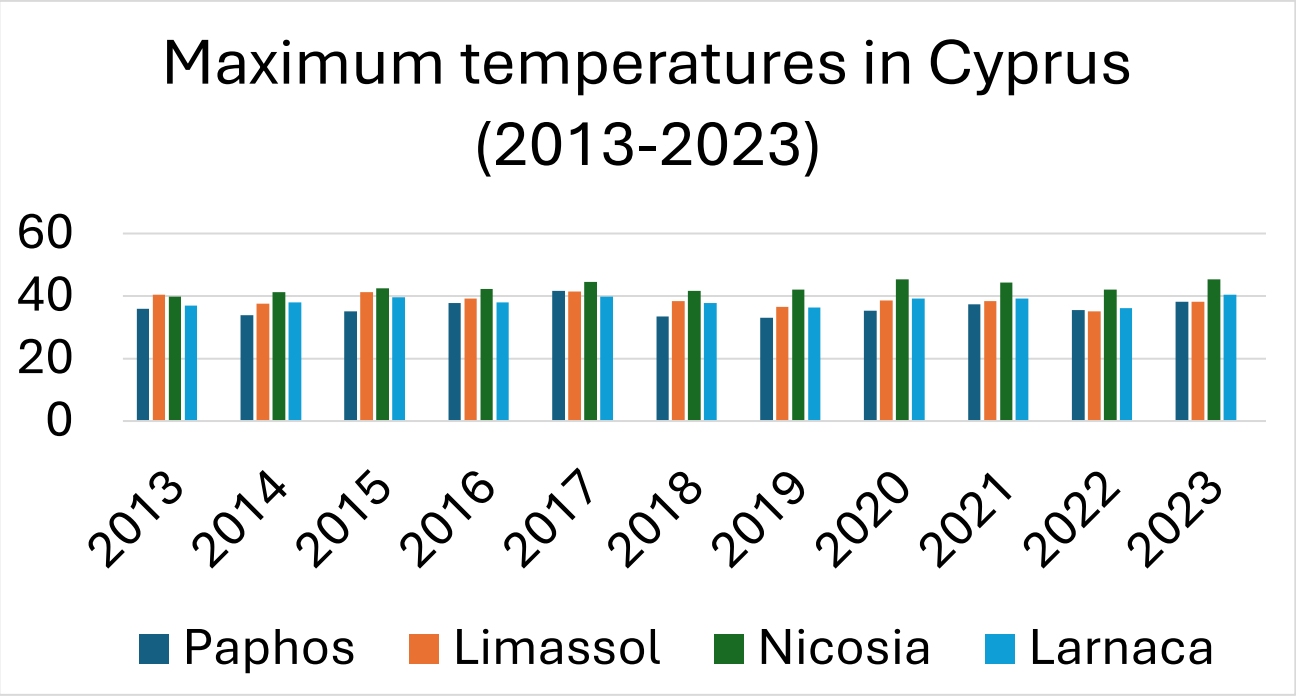

Fig. 2. Maximum temperatures observed in Cyprus' four major cities, during 2013-2023.

According to the time-series shown in Fig.3, is noticeable that Larnaca suffers the less by UHI phenomenon. On the other hand, a more steady trend observed in Limassol where *UHI* fluctuates between 0 and 1. Paphos after an extreme increase observed in summer of 2022 faced an extreme decrease of the phenomenon's intensity in 2023. In contrast, Nicosia in 2023 faced an extreme increase.

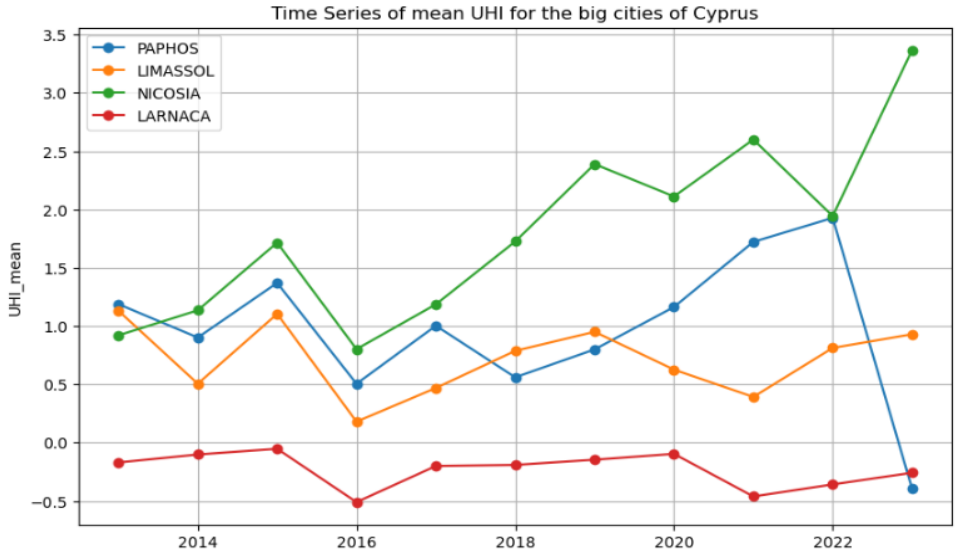

Fig. 3. Time-series of UHI for the four major cities' centers in Cyprus during 2013-2023.

Based on the temporal observations, shown in Fig. 4, done for the rural areas is easily recognized that Limassol's rural areas from 2016 to 2023 face less intense *UHI*. On the other hand, Paphos and Larnaca are facing some fluctuations of

such events in their rural areas, while both during 2023, reached the low levels of *UHI*, similar to Limassol. Nicosia's rural areas are facing the most intense *UHI* during the decade 2023.

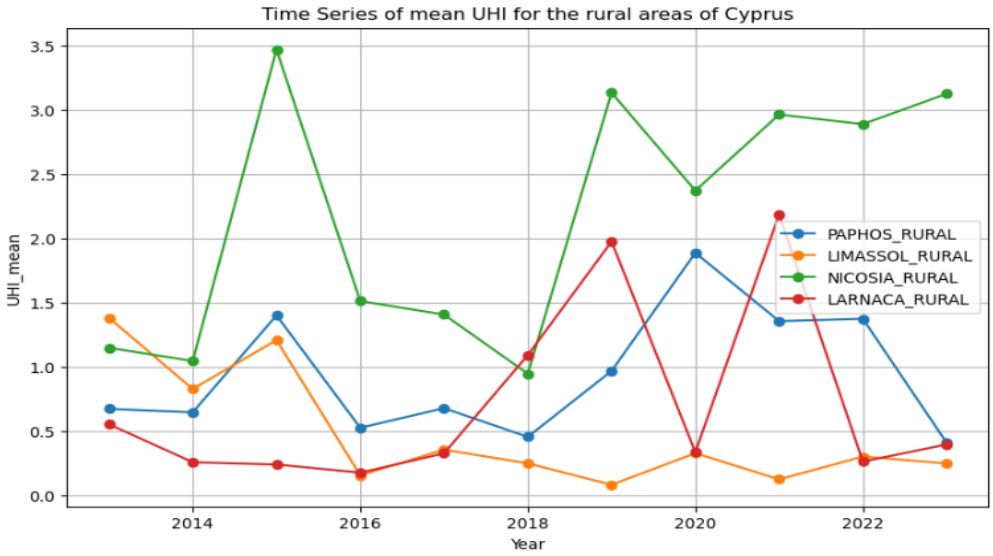

Fig. 4. Time-series of UHI for the four major cities' rural areas in Cyprus during 2013-2023.

Table 1 shows the results of the correlation analysis between *FVC* and *UHI*, as also as between *FVC* and *UTFVI*. Negative Pearson's and Spearman's correlations coefficients show that when the vegetation cover (*FVC*) both in rural areas of Cyprus and major cities' centres decreases, intense Urban Heat Island phenomena are observed. The same is true for the relationship between vegetation cover and Urban Thermal Field Variance Index (*UTFVI*). According to the differences of the two coefficients for the three out of four studied relationships, we can identify their non-linear status. On the other hand, the relationship *FVC-UTFVI* for the cities is linear.

Table 1. Pearson and Spearman correlation coefficient for the correlation between *FVC* and *UHI*, and the correlation between *FVC* and *UTFVI* at the major cities' centers and surrounding rural areas.

	Pearson		Spearman	
	FVC-UHI	*FVC-UTFVI*	*FVC-UHI*	*FVC-UTFVI*
Rural areas	-0.446	-0.382	-0.391	-0.372
Cities' center	-0.287	-0.214	-0.581	-0.214

4. CONCLUSION

In this work, a correlation analysis using Spearman and Pearson coefficients was conducted to understand the relations between vegetation coverage in cities and rural areas of Cyprus with *UHI* and the *UTFVI*. This analysis showed that the disappearance of green spaces in urban centers and the urbanization of rural areas through the years is leading to intense *UHI* in Cyprus. Furthermore, the intensification of *UTFVI* is also noted.

ACKNOWLEDGEMENTS

This work was conducted under the framework of the Ph.D. of the first author at the Cyprus University of Technology. The rest of the authors acknowledge the 'EXCELSIOR': ERATOSTHENES: EXcellence Research Centre for Earth

Surveillance and Space-Based Monitoring of the Environment H2020 Widespread Teaming project (www.excelsior2020.eu). The 'EXCELSIOR' project has received funding from the European Union's Horizon 2020 research and innovation programme under Grant Agreement No 857510 and from the Government of the Republic of Cyprus through the Directorate General for the European Programmes, Coordination and Development as well as the Cyprus University of Technology.

REFERENCES

[1] R. Gluch, D. A. Quattrochi, and J. C. Luvall, 'A multi-scale approach to urban thermal analysis', *Remote Sensing of Environment*, vol. 104, no. 2, pp. 123–132, Sep. 2006, doi: 10.1016/j.rse.2006.01.025.

[2] D. Hadjimitsis *et al.*, 'Satellite and Ground Measurements for Studying the Urban Heat Island Effect in Cyprus', in *Remote Sensing of Environment - Integrated Approaches*, D. Hadjimitsis, Ed., InTech, 2013. doi: 10.5772/39313.

[3] Y. Zhang and J. Cheng, 'Spatio-Temporal Analysis of Urban Heat Island Using Multisource Remote Sensing Data: A Case Study in Hangzhou, China', *IEEE J. Sel. Top. Appl. Earth Observations Remote Sensing*, vol. 12, no. 9, pp. 3317–3326, Sep. 2019, doi: 10.1109/JSTARS.2019.2926417.

[4] G. Kaplan, 'Evaluating the roles of green and built-up areas in reducing a surface urban heat island using remote sensing data', *Urbani izziv*, vol. 2, no. 30, pp. 105–112, Dec. 2019, doi: 10.5379/urbani-izziv-en-2019-30-02-004.

[5] F. Cecinati *et al.*, 'Exploitation of ESA and NASA Heritage Remote Sensing Data for Monitoring the Heat Island Evolution in Chennai with the Google Earth Engine', in *IGARSS 2019 - 2019 IEEE International Geoscience and Remote Sensing Symposium*, Yokohama, Japan: IEEE, Jul. 2019, pp. 6328–6331. doi: 10.1109/IGARSS.2019.8898040.

[6] A. Liebowitz, E. Sebastian, C. Yanos, M. Bilik, R. Blake, and H. Norouzi, 'Urban Heat Islands and Remote Sensing: Characterizing Land Surface Temperature at the Neighborhood Scale', in *IGARSS 2020 - 2020 IEEE International Geoscience and Remote Sensing Symposium*, Waikoloa, HI, USA: IEEE, Sep. 2020, pp. 4407–4409. doi: 10.1109/IGARSS39084.2020.9324473.

[7] N. Li and X. Li, 'The Impact of Building Thermal Anisotropy on Surface Urban Heat Island Intensity Estimation: An Observational Case Study in Beijing', *IEEE Geosci. Remote Sensing Lett.*, vol. 17, no. 12, pp. 2030–2034, Dec. 2020, doi: 10.1109/LGRS.2019.2962383.

[8] Q. Weng, U. Rajasekar, and X. Hu, 'Modeling Urban Heat Islands and Their Relationship With Impervious Surface and Vegetation Abundance by Using ASTER Images', *IEEE Trans. Geosci. Remote Sensing*, vol. 49, no. 10, pp. 4080–4089, Oct. 2011, doi: 10.1109/TGRS.2011.2128874.

[9] M. Eliades *et al.*, 'Earth Observation in the EMMENA Region: Scoping Review of Current Applications and Knowledge Gaps', *Remote Sensing*, vol. 15, no. 17, p. 4202, Aug. 2023, doi: 10.3390/rs15174202.

[10] N. Gorelick, M. Hancher, M. Dixon, S. Ilyushchenko, D. Thau, and R. Moore, 'Google Earth Engine: Planetary-scale geospatial analysis for everyone', *Remote Sensing of Environment*, vol. 202, pp. 18–27, Dec. 2017, doi: 10.1016/j.rse.2017.06.031.